

Incoherent self-accelerating beams

YAAKOV LUMER,¹ YI LIANG,^{2,3} RAN SCHLEY,¹ IDO KAMINER,¹ ELAD GREENFIELD,¹ DAOHONG SONG,² XINZHENG ZHANG,² JINGJUN XU,² ZHIGANG CHEN,^{2,4} AND MORDECHAI SEGEV^{1,*}

¹Physics Department, Technion–Israel Institute of Technology, Haifa 32000, Israel

²MOE Key Laboratory of Weak-Light Nonlinear Photonics, TEDA Applied Physics Institute & School of Physics, Nankai University, Tianjin 300457, China

³College of Physics Science and Technology, Guangxi University, Nanning 530004, China

⁴Department of Physics and Astronomy, San Francisco State University, San Francisco, California 94132, USA

*Corresponding author: msegev@technion.ac.il

Received 2 July 2015; revised 6 September 2015; accepted 6 September 2015 (Doc. ID 244204); published 9 October 2015

Self-accelerating optical beams form as a direct outcome of interference, initiated by a predesigned initial condition. In a similar fashion, quantum mechanical particles exhibit force-free acceleration as a result of interference effects following proper preparation of the initial Schrödinger wave function. Indeed, interference is at the heart of such wave packets, and hence it is implied that self-accelerating wave packets must be coherent entities. Counter to that, we demonstrate theoretically and experimentally spatially incoherent self-accelerating beams, in both the paraxial and the nonparaxial domains. We show that in principle, the transverse correlation distance can be as short as a single wavelength, while a properly designed initial beam will give rise to shape-preserving acceleration for the same distance as a coherent accelerating beam propagating on the same trajectory. These findings expand the understanding of the relation between coherence and accelerating beams, and may have implications for the design of self-accelerating quantum wave packets with limited quantum coherence. © 2015 Optical Society of America

OCIS codes: (030.4070) Modes; (050.1940) Diffraction; (350.5500) Propagation.

<http://dx.doi.org/10.1364/OPTICA.2.000886>

1. INTRODUCTION

The field of accelerating wave packets has attracted extensive research interest in the last several years, since the concept of Airy wave packets (first formulated in quantum mechanics [1]) was introduced into optics [2,3]. This acceleration, or self-bending—in the case of spatial acceleration—is first and foremost an effect of wave interference. In the regime of small angles (the paraxial domain), proper design of the initial amplitude and phase can generate a beam that propagates along a parabolic trajectory while maintaining a shape-preserving Airy profile. Such self-bending beams have led to many intriguing applications in the past several years, including particle manipulations [4,5], curved plasma channels [6], Airy plasmons [7–9], single-molecule imaging using the curved point-spread function [10], light-sheet microscopy using Airy beams [11], and even accelerating electron beams in electron microscopes [12]. The concept of accelerating beams was generalized to curved beams following arbitrary convex trajectories [13–17], and accelerating beams were shown to allow additional functional forms besides the Airy function [18]. Accelerating wave packets were also proposed [2] and demonstrated [19,20] in the temporal domain, where shape-preserving pulses accelerate for long distances in dispersive media (fibers) until causality causes their breakup [21]. Importantly, this concept was recently generalized to the full Maxwell equations [22], thereby enabling large bending angles close to 180° and features on the scale of a single wavelength [23–26]. This beyond-paraxiality generalization introduces a

wealth of additional accelerating trajectories [27–29]. Likewise, shape-preserving paraxial [30–32] and nonparaxial [33,34] self-accelerating beams were also found in nonlinear media, such as Kerr, saturable, and quadratic nonlinearities [31,35], and even in nonlocal nonlinear media [36]. Finally, accelerating beams were also found in nonhomogeneous landscapes such as waveguide arrays [37] and photonic crystals [38]. The past seven years of research on accelerating optical beams, together with the recent demonstration of accelerating electron beams that took the concept to the quantum domain [12], has proved that accelerating wave packets exist in a very broad range of wave systems.

In all of these systems where accelerating wave packets were explored, the underlying principle is wave interference, since the entire effect of acceleration is the direct outcome of this most basic property of waves of any kind. However, waves are not necessarily fully phase coherent. In fact, natural light sources are generally incoherent—because in most cases the emission of electromagnetic radiation results from spontaneous emission. In the quantum domain, incoherence is introduced by coupling to the environment, which inevitably causes dephasing and is generally perceived as disruptive to any quantum process. Can shape-preserving accelerating wave packets also occur in wave systems that are only partially coherent? Can they occur in systems where the coherence length is extremely short, comparable to a single wavelength?

Thus far, research on accelerating wave packets was focused on coherent beams. The most common method for creating paraxial

accelerating beams (Airy beams) is by shining the light through a cubic phase mask. Thus, the natural extension beyond coherent light would be to shine partially incoherent light through the same cubic phase mask, as indeed has been studied theoretically [39,40] and experimentally [41]. However, these few papers discussing self-accelerating beams using light that is not fully spatially coherent have treated imperfect coherence as a disruptive effect, claiming that the more incoherent a beam is, the shorter the range of its acceleration [39,41]. Those papers did not attempt to explain whether incoherence is indeed a fundamental limitation, but left the impression that incoherent shape-preserving accelerating beams are altogether impossible, due to the diminutive effects incoherence has on the propagation of such beams. Likewise, for other wave systems—from classical to quantum [12]—the lack of perfect coherence was always perceived as disruptive, and incoherent shape-preserving accelerating wave packets were thought to be impossible altogether.

Here, we investigate spatially partially incoherent shape-preserving accelerating beams, and demonstrate them theoretically and experimentally in both the paraxial and the highly nonparaxial regimes. We find that partial spatial coherence does not diminish the acceleration properties of the beam, provided that the beam is properly designed. Moreover, we show that it is possible to design accelerating beams with spatial transverse correlation distances as short as a single wavelength, and the beams still exhibit shape-preserving acceleration for the same distance as a coherent accelerating beam propagating on the same trajectory. Such highly incoherent accelerating beams display a single, broad intensity lobe and a smooth profile, instead of the highly oscillating one characteristic of all coherent accelerating beams. We provide explicit criteria for maintaining the acceleration despite the incoherence, and suggest applications, such as particle manipulation along curved paths [4,5,26], that could benefit greatly when the bending beams are partially incoherent. Finally, these findings may be beneficial for the design of self-accelerating quantum wave packets with limited quantum coherence.

2. THEORETICAL BACKGROUND

A. Spatial Incoherence

We begin by formulating the coherent-mode representation of partially spatially incoherent quasimonochromatic beams [42]. We write the electric field as $E(\vec{r}, t) = \text{Re}(U(\vec{r}, t)e^{i\omega t})$, where ω is the optical frequency and $U(\vec{r}, t)$ is an envelope that fluctuates much slower than the optical frequency. In this modal theory, the field $U(\vec{r}, t)$ can always be decomposed into a sum of statistically independent orthogonal modes, written as

$$U(\vec{r}, t) = \sum_n c_n(t) \psi_n(\vec{r}), \quad (1)$$

where $U(\vec{r}, t)$ is the randomly fluctuating field, $\psi_n(\vec{r})$ are the orthogonal modes that must satisfy boundary conditions in the medium, and $c_n(t)$ are randomly fluctuating complex coefficients, obeying $\langle c_n^*(t) c_{n'}(t) \rangle = a_n \delta_{nn'}$, with a_n having real values representing the power associated with each mode and $\langle \cdot \rangle$ indicating time averaging over times longer than the characteristic fluctuation time. The coherence function, defined as $W(\vec{r}_1, \vec{r}_2) = \langle U^*(\vec{r}_1, t) U(\vec{r}_2, t) \rangle$, can now be written as

$$W(\vec{r}_1, \vec{r}_2) = \sum_n a_n \psi_n^*(\vec{r}_1) \psi_n(\vec{r}_2). \quad (2)$$

A fully coherent beam is comprised of a single spatial mode, while a partially incoherent beam is comprised of an arbitrary number of modes. The intensity of the beam is then written as $I(\vec{r}) = W(\vec{r}, \vec{r}) = \sum_n a_n |\psi_n(\vec{r})|^2$, and the spatial correlation function is $\mu(\vec{r}_1, \vec{r}_2) = \frac{W(\vec{r}_1, \vec{r}_2)}{\sqrt{I(\vec{r}_1)} \sqrt{I(\vec{r}_2)}}$. The characteristic features of the partially spatially incoherent beam are determined by the properties of the modes $\psi_n(\vec{r})$. For example, with broad incoherent beams, a common model is to use plane waves as the independent modes, and the spatial spectrum of such plane waves then determines the coherence length. Another commonly used model is the Gaussian Schell-model [42], in which the modes used are Hermite–Gaussian modes. It is important to note that the expansion of Eqs. (1) and (2) can also be written using nonorthogonal modes, provided each mode $\psi_n(\vec{r})$ obeys the Helmholtz equation individually and that the coefficients c_n are without correlation.

B. Self-Accelerating Beams

We proceed by recalling the accelerating solutions of Maxwell's equations [22]. In vacuum, the time-harmonic electric field obeys the Helmholtz equation:

$$\nabla^2 \vec{E} + k^2 \vec{E} = 0, \quad (3)$$

where k is the wavenumber. The accelerating solution for the Helmholtz equation was shown to move along a circular trajectory [22]. For a TE-polarized electric field, $\vec{E} = E_y(x, z)\hat{y}$ can be written as

$$E_y(x, z) = \int_{-k}^k \frac{e^{i\alpha \sin^{-1}(k_x/k)}}{\sqrt{1 - (k_x/k)^2}} e^{ik_x x} e^{iz\sqrt{k^2 - k_x^2}} dk_x, \quad (4)$$

where k is the wavenumber and α is a (real) parameter determining the radius of the main lobe of the field via $r \approx \frac{\alpha}{k}$. The intensity profile of the field with $\lambda = 0.532 \mu\text{m}$ and $\alpha = 800$ is shown in Fig. 1(a). In the paraxial regime, one can write $E(x, y, z) = \psi(x, y, z)e^{-ikz}$ and approximate Eq. (3) by using the slowly varying envelope approximation $|\frac{\partial^2 \psi}{\partial z^2}| \ll |2k \frac{\partial \psi}{\partial z}|$, leading to the paraxial wave equation,

$$i \frac{\partial \psi}{\partial z} = \frac{1}{2k} \nabla_{\perp}^2 \psi, \quad (5)$$

which is formally equivalent to the Schrödinger equation from quantum mechanics, for which accelerating solutions were first suggested [1]. The accelerating solution for the paraxial equation

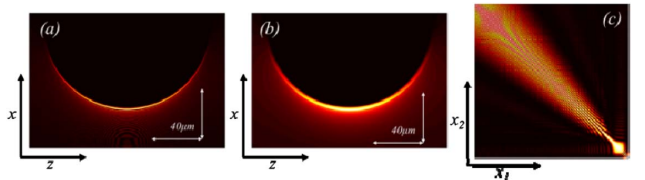


Fig. 1. Propagation dynamics of coherent and incoherent accelerating beams at wavelength $\lambda = 532 \text{ nm}$. (a) Propagation of a coherent nonparaxial accelerating beam with radius parameter $\alpha = 800$. The width of the main lobe is approximately $2 \mu\text{m}$. (b) Propagation of an incoherent nonparaxial accelerating beam with the radius parameter uniformly distributed in the range $\alpha \in [784, 816]$. The calculated bending angle in both cases is 160° , and the width of the main lobe is approximately $9 \mu\text{m}$. (c) Spatial correlation function $|\mu(x_1, x_2)|^2$ at $z = 0$ for the incoherent beam presented in (b). The spatial correlation distance at $z = 0$ is calculated to be $l_c \approx 2 \mu\text{m}$.

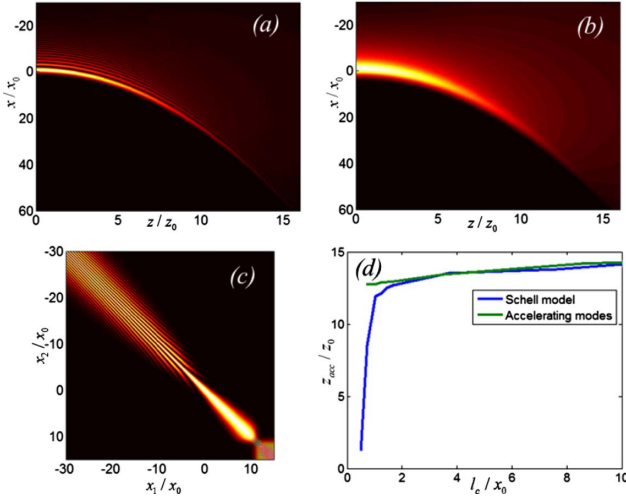


Fig. 2. Finite-size effects on coherent and incoherent accelerating beams. (a) Propagation of a coherent paraxial accelerating beam with an exponential truncation factor of $a = 0.03$, (b) propagation of an incoherent paraxial accelerating beam with exponential truncation factor of $a = 0.03$ and transverse correlation distance of $l_c \approx 1.5x_0$ at $z = 0$. The incoherent beam is described by the Gaussian Schell-model of Eq. (9). (c) Spatial correlation function $|\mu(x_1, x_2)|^2$ at $z = 0$ for the incoherent beam presented in (b); (d) acceleration distance z_{acc} versus coherence length l_c for paraxial incoherent beams, with $a = 0.03$, for beams obeying the Schell model (blue) and for beams constructed by the modal decomposition of Eq. (8) (green). In the coherent case, $z_{acc} = 15z_0$. In the Schell beams the acceleration dynamics deteriorates only when l_c is on the order of $1.5x_0$, which corresponds to one half of the main lobe. The incoherent beam generated using modes that accelerate along the same trajectory continues to accelerate even though the coherence length is smaller than x_0 .

is the Airy beam [2], which moves along a parabolic trajectory. The ideal nondiffracting Airy solution carries infinite power. However, one can truncate the ideal solution and obtain a finite-power solution, which accelerates for a finite distance [2,3]. We can write this accelerating solution using dimensionless variables $\tilde{x} = x/x_0$ and $\tilde{z} = z/(x_0^2 k)$:

$$\tilde{\psi}(\tilde{x}, \tilde{z}) = \text{Ai}\left(\tilde{x} - \left(\frac{1}{2}\tilde{z}\right)^2 - ia\tilde{z}\right) \times \exp\left(a\tilde{x} - \frac{1}{2}a\tilde{z}^2 + \frac{1}{12}i\tilde{z}^3 - \frac{1}{2}ia^2\tilde{z} - \frac{1}{2}i\tilde{z}\tilde{x}\right), \quad (6)$$

where x_0 is a characteristic width of the main lobe of the Airy beam and a is an exponential truncation factor. The accelerating trajectory, in real units, is $x = z^2/4x_0^3 k^2$. The intensity profile of such a beam is shown in Fig. 2(a). It is important to note that the spatial spectrum of the wave in Eq. (6) is Gaussian-shaped and has a cubic phase [2,3].

3. INCOHERENT SELF-ACCELERATING BEAMS: USING ACCELERATING MODES

A. Theory

Next, we construct partially spatially incoherent accelerating beams from these paraxial and nonparaxial solutions [Eqs. (6) and (4), respectively]. Based on the coherent mode representation of the coherence function [Eq. (2)], it is clearly seen that if

only some of the modes are accelerating while the others do not accelerate, then the entire incoherent beam will exhibit weaker acceleration properties (i.e., weaker acceleration and shorter acceleration range). Similarly, if all the modes are accelerating but they do it along different curves, the acceleration of the entire beam will be washed out and once again the beam will exhibit weaker acceleration properties. Therefore, we reason that in order for an incoherent beam to accelerate at a rate and a range equivalent to that of a coherent beam, the incoherent beam must be comprised strictly of modes that accelerate along the same curve. In the nonparaxial regime, such an accelerating incoherent beam should be constructed from stochastically populated modes that accelerate along the same circular trajectory with the same origin, but have different values of the radius parameter α , resulting in a beam comprised of a set of concentric rings:

$$E(x, z = 0, t) = \sum_n c_n(t) E_n(x, z = 0) = \sum_n c_n(t) \int_{-k}^k \frac{e^{i\alpha_n \sin^{-1}(k_x/k)}}{\sqrt{1 - (k_x/k)^2}} e^{ik_x x} dk_x. \quad (7)$$

The acceleration in the nonparaxial regime can persist for large angles, even when the transverse coherence length, defined as $l_c(\tilde{x}) = \int_{-\infty}^{\infty} |\mu(\tilde{x} - \frac{1}{2}\Delta x, \tilde{x} + \frac{1}{2}\Delta x)|^2 d\Delta x$ [42], is on the order of a single wavelength [see Figs. 1(b) and 1(c)]. Importantly, such an incoherent accelerating beam takes advantage of the fact that nonparaxial accelerating beams allow a family of solutions accelerating on the very same trajectory [22]—circles with different radii. In the paraxial regime, we construct the incoherent paraxial accelerating beam from stochastically populated parallel modes, where all the modes have the same acceleration (determined by x_0) but are differently shifted in x . Thus, this beam at $z = 0$ is

$$\psi(x, z = 0, t) = \sum_n c_n(t) \psi_n(x, z = 0) = \sum_n c_n(t) \text{Ai}\left(\frac{x - \Delta_n}{x_0}\right) e^{a(x - \Delta_n)/x_0}, \quad (8)$$

where Δ_n is a series of arbitrary shifts (real numbers) that are not necessarily equally spaced. Thus, the intensity patterns of such (nonparaxial and paraxial) beams accelerate with the same acceleration properties (rate and range) as a single accelerating mode does. This behavior persists even when the transverse coherence length l_c is smaller than the width of the main lobe of a coherent beam, which we estimate to be $\sim 3x_0$ [see Fig. 2(d)]. We would like to highlight what happens when the chosen modes are not accelerating along the same trajectory, which happens, for example, in Eq. (8) due to the different x_0 values for different modes. Under such conditions, the acceleration of the beam suffers dramatically because the shape-preserving property does not persist. An illustrative example is presented in Supplement 1. The modes presented in Eqs. (7) and (8) are not orthogonal. However, as stated earlier, the modal expansion of Eqs. (1) and (2) is valid even in the case of nonorthogonal modes, provided each mode obeys the Helmholtz equation. The way to see this is to write the coherence function $W(x_1, x_2) = \langle U^*(x_1, t) U(x_2, t) \rangle$ using the modes in Eqs. (7) and (8), and then to recast $W(x_1, x_2)$ into an orthogonal-mode decomposition, akin to Eq. (2) by diagonalization. In this way, it can be easily seen that the intensity pattern for each z is the sum of the intensities of the modes in Eqs. (7) and (8), without interference among modes. It is important to note that

when the range of c_n values that have appreciable amplitudes becomes larger and larger, the coherence length l_c decreases, and with it the width of the main lobe increases. Clearly, at the extreme case of a very small l_c and very large width of the main lobe, acceleration along finite angles or finite distance carries little significance. However, the interesting cases are the intermediate ones, and these are the ones that are discussed in this paper.

B. Experiment

Experimental results with incoherent nonparaxial accelerating beams are presented in Fig. 3. The experimental system is depicted in Fig. 3(a). Laser light with a wavelength of $\lambda = 532$ nm is used. A spatial light modulator (SLM) imposes the appropriate phase profile for generating nonparaxial accelerating beams [22], and two objective lenses (X60, NA = 0.85) focus the accelerating beam to the micrometer scale. By moving one of the objective lenses, we image the intensity pattern at different planes and thus map out the acceleration trajectory of the beam. Experimentally, we first generate a coherent nonparaxial accelerating beam, with the radius parameter $\alpha = 800$. This beam bends on a circular trajectory, over an angle of approximately 65° , which is highly nonparaxial, as presented in Fig. 3(b). Next, we generate an incoherent beam where all the modes comprising it accelerate along the same trajectory, as described by Eq. (7). We do so by alternating among multiple phase profiles imposed on the

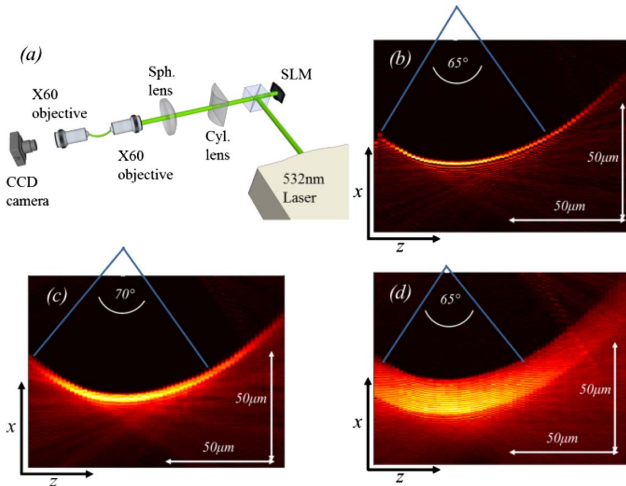


Fig. 3. Experiments with partially spatially incoherent accelerating beams. (a) Experimental setup. A laser beam of wavelength 532 nm is reflected from an SLM that imposes the appropriate phase profile. When the SLM alternates among these phase profiles faster than the integration time of our camera, the camera measures only the time-average intensity distribution. A cylindrical lens Fourier transforms the beam, which is tightly focused and imaged into a CCD camera using two objective lenses (X60, NA = 0.85). (b) Measured propagation dynamics of a coherent nonparaxial accelerating beam, with radius parameter $\alpha = 800$. The bending angle is $\approx 65^\circ$, and width of the main lobe is approximately $2 \mu\text{m}$. (c),(d) Measured propagation dynamics of two examples of incoherent nonparaxial accelerating beams, generated by temporally modulating the phase profiles on the SLM corresponding to the radius parameters in the ranges $\alpha \in [786, 816]$ and $\alpha \in [730, 880]$, respectively. The beams in both examples consist of 16 modes. The beam in (c) has a bending angle of $\approx 70^\circ$ and width of the main lobe of approximately $10 \mu\text{m}$, with a transverse correlation distance at $z = 0$ of $l_c \approx 2 \mu\text{m}$, while the beam in (d) has a bending angle of $\approx 65^\circ$ and width of the main lobe of approximately $20 \mu\text{m}$, with a transverse correlation distance at $z = 0$ of $l_c \approx 0.7 \mu\text{m}$.

SLM, each of which is properly designed to launch a single accelerating beam with a given α parameter. When the SLM alternates among these phase profiles (at 16 Hz) faster than the integration time of our camera (1 Hz), the camera measures only the time-averaged intensity distribution. This measured time-averaged intensity is equal to the intensity distribution of an incoherent beam constructed from exactly the same modal structure. This is due to the fact that for incoherent light the interference among modes is washed out because their fluctuating populations $c_n(t)$ are uncorrelated. Likewise, in our experimental realization the interference among modes is nonexistent because the modes alternate, never coexisting within the same time window. However, because all the modes are accelerating along the same trajectory, the lack of coherence does not hamper the acceleration. We present two examples of nonparaxial accelerating incoherent beams, both consisting of 16 modes. The first is presented in Fig. 3(c), with α spanning from 786 to 816. It can be seen in Fig. 3(c) that the beam bends over an angle of approximately 70° , which is even larger than the coherent case, while maintaining a beam profile that is smooth and without the oscillations that are an inherent part of any accelerating coherent beam. The coherence length at $z = 0$ is calculated to be $l_c \approx 2 \mu\text{m}$. The second example is presented in Fig. 3(d), with α spanning from 730 to 880. In this case, the main lobe is very thick, and the coherence length at $z = 0$ is calculated to be $l_c \approx 0.7 \mu\text{m}$, which is about 1.4λ . The beam in the second example accelerates over an angle of α , which is the same as the coherent beam generated using similar parameters. Thus, we have experimentally demonstrated an incoherent nonparaxial accelerating beam with a coherence length on the order of a single wavelength.

4. INCOHERENT SELF-ACCELERATING BEAMS: USING LIGHT FROM ROTATING DIFFUSER

A. Theory

Having demonstrated how to engineer a highly incoherent accelerating beam, the next natural question would be: is it possible to accelerate a beam of natural incoherent light? To answer that, we analyze the features of quasimonochromatic, spatially incoherent accelerating beams generated, for example, with a rotating diffuser [43,44], or from spectrally filtered sunlight passed through a pinhole [45]. We analyze such beams in the paraxial regime, and model them using the Gaussian Schell model [42], in which the spatial coherence between two points is a Gaussian function of the distance between them. A similar treatment was presented for the case of nondiffracting incoherent Bessel beams [46]. For simplicity, we focus on one-dimensional beams, but our results apply equally well to two-dimensional cases. Using a beam with a Gaussian intensity profile, we can write the coherence function at the Fourier plane [42,43]:

$$W(k_1, k_2) = I_0 \exp\left(-\frac{(k_1 - k_2)^2}{2\sigma^2}\right) \times \exp\left(-\frac{(k_1^2 + k_2^2)}{w^2} - \frac{i}{3}c_0^3(k_1^3 - k_2^3)\right) \quad (9)$$

where k_1 and k_2 are the spatial coordinates in the Fourier plane, w is the width of the intensity structure of the beam at the Fourier plane, σ is the width of the spatial correlation function, c_0 is the coefficient of the cubic phase profile, and I_0 is the peak intensity. In this representation, a coherent, finite-energy accelerating Airy

beam is described by Eq. (9) with $\sigma \rightarrow \infty$. Experimentally, such an incoherent accelerating paraxial beam is generated by passing a laser beam through a rotating diffuser, which naturally forms the beam described by Eq. (9), and subsequently passing the beam through a mask (e.g., the SLM) displaying the proper cubic phase profile positioned at the Fourier plane of the beam. The intensity pattern of such an incoherent accelerating beam [obtained by the Fourier transform of Eq. (9)] is presented in Fig. 2(b). The spatial correlation function $\mu(x_1, x_2)$ at $z = 0$ is shown in Fig. 2(c). Recalling that ideal Airy beams are not square integrable and thus the finite-energy solution accelerates in a shape-preserving fashion only for a finite distance z_{acc} , it is essential to study the effect of incoherence on z_{acc} . We define z_{acc} as the distance in which the peak intensity ceases to follow the parabolic trajectory prescribed by Eq. (6). Analyzing the effect of incoherence on z_{acc} , we reach the following surprising conclusion, illustrated in Fig. 2(d): even highly incoherent beams can still exhibit significant acceleration, similar to their coherent counterparts. The acceleration distance z_{acc} is only weakly dependent upon the coherence properties of the beam, as long as the transverse coherence length l_c is larger than approximately half the width of the main lobe of the equivalent coherent beam. Only when l_c is smaller than half the width of the main lobe is the acceleration distance decreased significantly, as is shown in Fig. 2(d). This highly surprising behavior can be explained by making note that the coherence function described by Eq. (9) can be decomposed into modes, according to Eq. (2). These modes are in this case Hermite–Gauss modes with a cubic phase profile, and the power associated with each mode decreases exponentially. As is seen in [2,3], the coherent finite energy Airy beam is the Fourier transform of a Gaussian with a cubic phase. When the cubic phase profile is imposed on a higher-order Gaussian, the main lobe of the beam still accelerates, but a certain amount of power is diffracted away due to the nodes in the spectrum. We elaborate on the characteristic features of accelerating beams generated using higher-order modes instead of a simple Gaussian beam and discuss the way they affect the overall dynamics of the incoherent accelerating beam in Supplement 1.

B. Experiment

We now present the experimental results with incoherent paraxial accelerating beams. The experimental setup is sketched in Fig. 4(a). The incoherent beam is obtained by passing a 532 nm laser beam through a rotating diffuser. The beam is then reflected from the SLM, where the cubic phase pattern is imposed, thus achieving the form of Eq. (9). A Fourier transforming lens is placed to obtain the incoherent accelerating beam, such that $x_0 = 75 \mu\text{m}$ and the truncation parameter is $a = 0.075$. To enable proper comparison with coherent accelerating beams, we first present the propagation of a coherent accelerating beam. The initial beam and the beam at propagation distance $z = 20 \text{ cm}$ are shown in Figs. 4(b) and 4(c), respectively. Figure 4(h) shows the corresponding side view of the propagation, where the bending of the main lobe is clearly visible. Next, we present two examples of accelerating beams with incoherent light. In the first example, the transverse coherence length at $z = 0$ is $l_c = 215 \mu\text{m}$, and the initial beam and the beam at propagation distance $z = 20 \text{ cm}$ are shown in Figs. 4(d) and 4(e), respectively. Figure 4(i) shows the corresponding side view of the propagation, where the bending of the main lobe is again clearly visible, despite the obvious fact that the intensity oscillations of the beam are

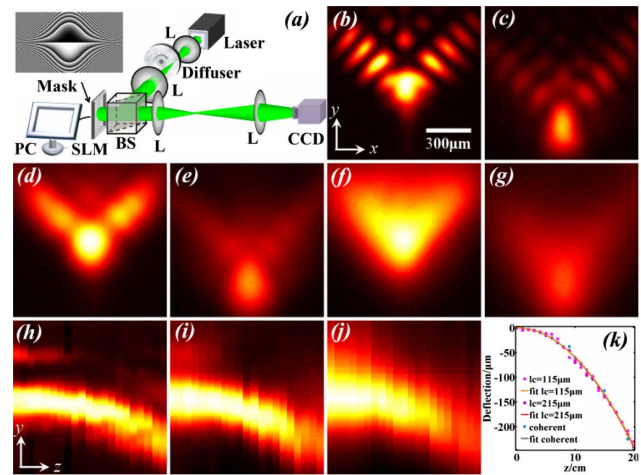


Fig. 4. Experiments with two-dimensional incoherent paraxial accelerating beams. (a) Experimental setup, where L stands for lens and BS for beamsplitter. The incoherent beam is generated by a rotating diffuser followed by an SLM, with $x_0 = 75 \mu\text{m}$ and $a = 0.075$. (b)–(g) Transverse intensity patterns taken at propagation distance $z = 0$ [(b), (d), (f)] and at $z = 20 \text{ cm}$ [(c), (e), (g)] for a coherent Airy beam [(b), (c)], an incoherent Airy beam with $l_c \approx 215 \mu\text{m}$ [(d), (e)], and an incoherent accelerating beam with $l_c \approx 115 \mu\text{m}$ [(f), (g)]; (h)–(j) side view of beam propagation for the three cases (coherent, $l_c \approx 215 \mu\text{m}$, $l_c \approx 115 \mu\text{m}$), respectively; (k) deflection of the main lobe of the accelerating beams as a function of propagation distance for the three cases. It is evident that the incoherence does not affect the acceleration for the distances presented.

smear. The smearing is even more pronounced in the second example with $l_c = 115 \mu\text{m}$, which is on the order of about half the width of the main lobe of the coherent beam. The initial beam and the beam at propagation distance $z = 20 \text{ cm}$ are shown in Figs. 4(f) and 4(g), respectively. Figure 4(j) shows the corresponding side view of the propagation. The deflection of the main lobe is again clearly visible, despite the complete lack of the intensity oscillations. That is, this incoherent accelerating beam has no sidelobes whatsoever, in sharp contrast with coherent accelerating beams where the acceleration (beam bending) is created by the oscillating structure of the beam. The results are summarized in Fig. 4(k), where the deflection of the main lobe versus the propagation distance is plotted. According to our estimates, in both the coherent and incoherent cases the acceleration dynamics breaks down at $z \approx 70 \text{ cm}$, which is outside our experimental regimes. Nevertheless, our experimental results clearly demonstrate that despite significant incoherence and even when the transverse coherence length l_c can be on the order of one half the width of the main lobe, the acceleration dynamics persists in the same way as in the fully coherent case.

5. CONCLUSIONS

In conclusion, we have presented, experimentally and theoretically, incoherent accelerating beams, in both the nonparaxial and the paraxial regimes. We have shown that by constructing the incoherent beam solely of modes that accelerate along the same trajectory, the incoherence does not hamper the acceleration. We demonstrated experimentally incoherent nonparaxial beams with a transverse coherence length on the order of a single

wavelength, which accelerate up to the same bending angle as their coherent counterparts with similar parameters. We demonstrated how to engineer such beams using temporal modulation of the phase mask, a technique that will be useful for all applications where the natural response time is slower than the modulation speed—for example, particle manipulation along curved paths. In addition, we analyzed incoherent accelerating beams generated using natural light, and have shown, theoretically and experimentally, that for a wide range of parameters the incoherence of the beam does not hamper its acceleration properties. Our work provides a new outlook for the field of accelerating beams, no longer treating incoherence as a disruptive effect, but rather expanding the scope of beam acceleration to incoherent wave packets. Finally, the concept presented here also applies to accelerating wave packets outside the domain of optics, for example, accelerating electron beams, accelerating ion beams, and accelerating beams of cold atoms, where incoherence often poses major challenges.

Funding. I-CORE Israeli Center of Excellence “Circle of Light”; U.S. - Israel Binational Science Foundation (BSF); Israel Science Foundation; Marie Curie (328853–MC–BSiCS); National Key Basic Research Program (2013CB328702, 2013CB632703); National Natural Science Foundation of China (NSFC) (11304165); 111 Project of China (B07013); PCSIRT (IRT0149); National Science Foundation (NSF); Army Research Office.

See [Supplement 1](#) for supporting content.

REFERENCES

- M. V. Berry and N. L. Balazs, “Nonspreading wave packets,” *Am. J. Phys.* **47**, 264–267 (1979).
- G. A. Siviloglou and D. N. Christodoulides, “Accelerating finite energy Airy beams,” *Opt. Lett.* **32**, 979–981 (2007).
- G. A. Siviloglou, J. Broky, A. Dogariu, and D. N. Christodoulides, “Observation of accelerating Airy beams,” *Phys. Rev. Lett.* **99**, 213901 (2007).
- J. Baumgartl, M. Mazilu, and K. Dholakia, “Optically mediated particle clearing using Airy wavepackets,” *Nat. Photonics* **2**, 675–678 (2008).
- P. Zhang, J. Prakash, Z. Zhang, M. S. Mills, N. K. Efremidis, D. N. Christodoulides, and Z. Chen, “Trapping and guiding microparticles with morphing autofocusing Airy beams,” *Opt. Lett.* **36**, 2883–2885 (2011).
- P. Polynkin, M. Kolesik, J. V. Moloney, G. A. Siviloglou, and D. N. Christodoulides, “Curved plasma channel generation using ultraintense Airy beams,” *Science* **324**, 229–232 (2009).
- A. Minovich, A. E. Klein, N. Janunts, T. Pertsch, D. N. Neshev, and Y. S. Kivshar, “Generation and near-field imaging of Airy surface plasmons,” *Phys. Rev. Lett.* **107**, 116802 (2011).
- P. Zhang, S. Wang, Y. Liu, X. Yin, C. Lu, Z. Chen, and X. Zhang, “Plasmonic Airy beams with dynamically controlled trajectories,” *Opt. Lett.* **36**, 3191–3193 (2011).
- L. Li, T. Li, S. M. Wang, C. Zhang, and S. N. Zhu, “Plasmonic Airy beam generated by in-plane diffraction,” *Phys. Rev. Lett.* **107**, 126804 (2011).
- S. Jia, J. C. Vaughan, and X. Zhuang, “Isotropic three-dimensional super-resolution imaging with a self-bending point spread function,” *Nat. Photonics* **8**, 302–306 (2014).
- T. Vettenburg, H. I. C. Dalgarno, J. Nytk, C. Coll-Lladó, D. E. K. Ferrier, T. Čížmár, F. J. Gunn-Moore, and K. Dholakia, “Light-sheet microscopy using an Airy beam,” *Nat. Methods* **11**, 541–544 (2014).
- N. Voloch-Bloch, Y. Lereah, Y. Lilach, A. Gover, and A. Arie, “Generation of electron Airy beams,” *Nature* **494**, 331–335 (2013).
- E. Greenfield, M. Segev, W. Walasik, and O. Raz, “Accelerating light beams along arbitrary convex trajectories,” *Phys. Rev. Lett.* **106**, 213902 (2011).
- L. Froehly, F. Courvoisier, A. Mathis, M. Jacquot, L. Furfaro, R. Giust, P. A. Lacourt, and J. M. Dudley, “Arbitrary accelerating micron-scale caustic beams in two and three dimensions,” *Opt. Express* **19**, 16455–16465 (2011).
- I. D. Chremmos, Z. Chen, D. N. Christodoulides, and N. K. Efremidis, “Bessel-like optical beams with arbitrary trajectories,” *Opt. Lett.* **37**, 5003–5005 (2012).
- I. D. Chremmos and N. K. Efremidis, “Nonparaxial accelerating Bessel-like beams,” *Phys. Rev. A* **88**, 063816 (2013).
- Y. Hu, D. Bongiovanni, Z. Chen, and R. Morandotti, “Multipath multi-component self-accelerating beams through spectrum-engineered position mapping,” *Phys. Rev. A* **88**, 043809 (2013).
- M. A. Bandres, “Accelerating beams,” *Opt. Lett.* **34**, 3791–3793 (2009).
- A. Chong, W. H. Renninger, D. N. Christodoulides, and F. W. Wise, “Airy-Bessel wave packets as versatile linear light bullets,” *Nat. Photonics* **4**, 103–106 (2010).
- D. Abdollahpour, S. Sunstov, D. G. Papazoglou, and S. Tzortzakis, “Spatiotemporal Airy light bullets in the linear and nonlinear regimes,” *Phys. Rev. Lett.* **105**, 253901 (2010).
- I. Kaminer, Y. Lumer, M. Segev, and D. N. Christodoulides, “Causality effects on accelerating light pulses,” *Opt. Express* **19**, 23132–23139 (2011).
- I. Kaminer, R. Bekenstein, J. Nemirovsky, and M. Segev, “Nondiffracting accelerating wave packets of Maxwell’s equations,” *Phys. Rev. Lett.* **108**, 163901 (2012).
- F. Courvoisier, A. Mathis, L. Froehly, R. Giust, L. Furfaro, P. A. Lacourt, M. Jacquot, and J. M. Dudley, “Sending femtosecond pulses in circles: highly nonparaxial accelerating beams,” *Opt. Lett.* **37**, 1736–1738 (2012).
- I. Kaminer, E. Greenfield, R. Bekenstein, J. Nemirovsky, A. Mathis, L. Froehly, F. Courvoisier, and M. Segev, “Accelerating beyond the horizon,” *Opt. Photon. News* **23**(12), 26 (2012).
- A. Mathis, F. Courvoisier, L. Froehly, L. Furfaro, M. Jacquot, P. A. Lacourt, and J. M. Dudley, “Micromachining along a curve: femtosecond laser micromachining of curved profiles in diamond and silicon using accelerating beams,” *Appl. Phys. Lett.* **101**, 071110 (2012).
- R. Schley, I. Kaminer, E. Greenfield, R. Bekenstein, Y. Lumer, and M. Segev, “Loss-proof self-accelerating beams and their use in non-paraxial manipulation of particles’ trajectories,” *Nat. Commun.* **5**, 5189 (2014).
- P. Aleahmad, M.-A. Miri, M. S. Mills, I. Kaminer, M. Segev, and D. N. Christodoulides, “Fully vectorial accelerating diffraction-free Helmholtz beams,” *Phys. Rev. Lett.* **109**, 203902 (2012).
- P. Zhang, Y. Hu, T. Li, D. Cannan, X. Yin, R. Morandotti, Z. Chen, and X. Zhang, “Nonparaxial Mathieu and Weber accelerating beams,” *Phys. Rev. Lett.* **109**, 193901 (2012).
- M. A. Bandres, M. A. Alonso, I. Kaminer, and M. Segev, “Three-dimensional accelerating electromagnetic waves,” *Opt. Express* **21**, 13917–13929 (2013).
- J. A. Giannini and R. I. Joseph, “The role of the second Painlevé transcendent in nonlinear optics,” *Phys. Lett. A* **141**, 417–419 (1989).
- I. Kaminer, M. Segev, and D. N. Christodoulides, “Self-accelerating self-trapped optical beams,” *Phys. Rev. Lett.* **106**, 213903 (2011).
- A. Lotti, D. Faccio, A. Couairon, D. G. Papazoglou, P. Panagiotopoulos, D. Abdollahpour, and S. Tzortzakis, “Stationary nonlinear Airy beams,” *Phys. Rev. A* **84**, 021807 (2011).
- I. Kaminer, J. Nemirovsky, and M. Segev, “Self-accelerating self-trapped nonlinear beams of Maxwell’s equations,” *Opt. Express* **20**, 18827–18835 (2012).
- P. Zhang, Y. Hu, D. Cannan, A. Salandrino, T. Li, R. Morandotti, X. Zhang, and Z. Chen, “Generation of linear and nonlinear nonparaxial accelerating beams,” *Opt. Lett.* **37**, 2820–2822 (2012).
- I. Dolev, I. Kaminer, A. Shapira, M. Segev, and A. Arie, “Experimental observation of self-accelerating beams in quadratic nonlinear media,” *Phys. Rev. Lett.* **108**, 113903 (2012).
- R. Bekenstein and M. Segev, “Self-accelerating optical beams in highly nonlocal nonlinear media,” *Opt. Express* **19**, 23706–23715 (2011).
- R. El-Ganainy, K. G. Makris, M. A. Miri, D. N. Christodoulides, and Z. Chen, “Discrete beam acceleration in uniform waveguide arrays,” *Phys. Rev. A* **84**, 023842 (2011).
- I. Kaminer, J. Nemirovsky, K. G. Makris, and M. Segev, “Self-accelerating beams in photonic crystals,” *Opt. Express* **21**, 8886–8896 (2013).
- H. T. Eyyuboğlu and E. Sermtulu, “Partially coherent Airy beam and its propagation in turbulent media,” *Appl. Phys. B* **110**, 451–457 (2012).

40. Y. Dong, L. Zhang, J. Luo, W. Wen, and Y. Zhang, "Degree of paraxiality of coherent and partially coherent Airy beams," *Opt. Laser Technol.* **49**, 1–5 (2013).
41. J. E. Morris, M. Mazilu, J. Baumgartl, T. Cizmar, and K. Dholakia, "Propagation characteristics of Airy beams: dependence upon spatial coherence and wavelength," *Opt. Express* **17**, 13236–13245 (2009).
42. L. Mandel and E. Wolf, *Optical Coherence and Quantum Optics* (Cambridge University, 1995).
43. B. Crosignani, "Light scattering by a rotating disk," *J. Appl. Phys.* **42**, 399 (1971).
44. M. Mitchell, Z. Chen, M. Shih, and M. Segev, "Self-trapping of partially spatially incoherent light," *Phys. Rev. Lett.* **77**, 490–493 (1996).
45. M. Mitchell and M. Segev, "Self-trapping of incoherent white light," *Nature* **387**, 880–883 (1997).
46. J. Turunen, A. Vasara, and A. T. Friberg, "Propagation invariance and self-imaging in variable-coherence optics," *J. Opt. Soc. Am. A* **8**, 282–289 (1991).